Adsorption of Methyl Violet Dye From Wastewater Using Poly(Methacrylic Acid-co-acrylamide)/bentonite Nanocomposite Hydrogels

Hamid Safarzadeh
University of Tehran College of Engineering
Seyed Hamed Mousavi
University of Tehran College of Engineering
Seyed Jamaleddin Peighambardoust (j.peighambardoust@tabrizu.ac.ir)
University of Tabriz
Reza Mohammadi
University of Tabriz
Seyed Hadi Peighambardoust
University of Tabriz Faculty of Agriculture

Research Article

Keywords: Methacrylic acid-co-acrylamide copolymer, Nanocomposite hydrogel, Adsorption, Methyl Violet

Posted Date: July 20th, 2021

DOI: https://doi.org/10.21203/rs.3.rs-700381/v1

Version of Record: A version of this preprint was published at Journal of Polymer Research on March 8th, 2022. See the published version at https://doi.org/10.1007/s10965-022-02956-0.

Adsorption of methyl violet dye from wastewater using poly(methacrylic acid-co-acrylamide)/bentonite nanocomposite hydrogels

Hamid Safarzadeh[1], Seyed Hamed Mousavi[1*], Seyed Jamaleddin Peighambardoust[2**], Reza Mohammadi[3], Seyed Hadi Peighambardoust[4]

[1] Separation Processes & Nanotechnology Lab, Faculty of Caspian, College of Engineering, University of Tehran, Tehran, Iran

[2] Faculty of Chemical and Petroleum Engineering, University of Tabriz, Tabriz, 5166616471, Iran,

[3] Polymer Research Laboratory, Faculty of Chemistry, University of Tabriz, Tabriz, Iran

[4] Department of Food Science, College of Agriculture, University of Tabriz, Tabriz 5166616471, Iran

[*] Corresponding author email: mhmousavi@ut.ac.ir

[**] Corresponding author email: j.peighambardoust@tabrizu.ac.ir

Abstract

One of the major environmental problems is the entry of colored pollutants into the oceans and seas. Adsorption is one of the effective methods to eliminate colorant polluting materials from wastewater streams. In this study, nanocomposite hydrogels of poly(methacrylic acid-co-acrylamide) (Poly(MAA-co-AAm)) containing different weight percent bentonite clay nanoparticles (0, 5, 10, and 15 wt. %) were used to remove methyl violet (MV) dye. FTIR, SEM, TGA, and XRD were used to analyze the properties of adsorbents. Results showed that bentonite nanoparticles were successfully distributed in the hydrogel system. Bentonite nanoparticles at 10 wt. % gave the maximum MV dye adsorption efficiency. The highest adsorption was obtained at a pH of 5, an adsorbent dosage of 1.5 g/L, a temperature of 25°C, a contact time of 60 min, and a pollutant concentration of 10 mg/L. In thermodynamics studies, a negative values of Gibbs free energy (ΔG°) indicating that the adsorption process was spontaneous. In addition, Poly(MAA-co-AAm) hydrogels and Poly(MAA-co-AAm)/bentonite nanocomposite hydrogels gave the adsorption enthalpy (ΔH°) of 22.2 and 47.4 KJ/mol. Langmuir isotherm model was successfully applied in describing the equilibrium behavior of the adsorption process. To investigate the adsorption kinetics, we used pseudo-first-order, pseudo-second-order, and Elovich models. The kinetic study showed that the pseudo-second-order model was more successful in describing the kinetic behavior of the adsorption process than pseudo-first-order and Elovich models. Incorporating bentonite clay nanoparticles in Poly(MAA-co-AAm) nanocomposite hydrogels significantly improved the adsorption and swelling efficiencies of these hydrogels.

Keywords: Methacrylic acid-co-acrylamide copolymer, Nanocomposite hydrogel, Adsorption, Methyl Violet

1. Introduction

Water pollution from the improper discharge of industrial dyes originated from various industries such as textile, leather, paper, plastic, tanning, etc. is a very serious environmental concern, which threaten the living organisms and ecosystem [1,2]. It is, therefore, necessary to remove these toxic pollutants from industrial effluents before discharging to the environment. Dyes are one of the most important groups of the pollutants [3,4] and are usually classified into cationic (basic), anionic (direct, acidic, and reactive), and non-ionic [5,6] types. The annual production of industrial dyes is estimated to be 10,000 tons, of which about 1 to 10 percent of is being discharged to the environment [7]. Complete removal of dyes from the wastewater streams is a challenging issue because of their longer stability in the environment. In previous studies various techniques such as electrochemical, ion exchange, catalysis, deformation, adsorption and biological processes have been proposed to remove the dyes from aqueous solutions [8,9]. Water treatment systems based on hydrogel show the potential of efficient adsorption due to the three-dimensional network of polymer chains and hydrophilic nature of hydrogels [10]. In addition, hydrogels have the advantage of being cheap, non-toxic, chemically and physically stable, forming a good polymer network, and ability to recycle [11,12]. Hydrogels exhibit a high adsorption affinity to remove different chemicals from aqueous solutions even at lower concentrations, which makes them important for widespread use in environmental applications [13,14]. Common functional groups used in the synthesis of hydrogels include carboxylic acids, amides, amines, hydroxyl, and sulfonic acids. Highly adsorbable hydrogels swell due to the penetration of water at pre-existing or dynamically spaced distances between polymer chains [15]. In the structure of monomers, there is an acidic group -COOH, which plays an important role in the adsorption and swelling properties of hydrogels. These monomers are present in the hydrogel structure in the form of copolymer bonds and frequently alter molecular chain experiences, hydrophobicity, response to stimuli, therapeutic behaviors, and the allowable amount of hydrogel [16]. Due to the presence of oxygen atoms, acrylics form complexes with metal cations and cationic dyes [17]. In addition, hydrogen bonds between polymer chains, water molecules and dyes are formed due to the presence of the -OH group. Due to the weak acidity of the carboxylic group, the hydrogel behavior of acrylic

patients is sensitive to pH [18]. In the adsorption process, various materials such as agricultural waste, natural polymers (chitin, chitosan, carboxy methylcellulose, etc.), silicate layers such as mineral clays and activated carbon may be used as adsorbents to remove certain chemicals from wastewaters [19]. Clay is a low-cost, biocompatible and abundant material with good mechanical and chemical properties, which can be used in the concept of wastewater treatment [20,21]. Bentonite nanoclay is one of the clay minerals that form Smectite family materials which is composed of two silica tetrahedral sheets with a central octahedral sheet and are designated as 2:1 layer mineral, and water molecules and cations occupying the space between the 2:1 layers. Bentonite is used to remove organic dyes due to its high surface area and cation-exchange ability [22,23]. The aim of this study was to synthesize and characterize Poly(MAA-co-AAm)/bentonite nanocomposite hydrogels as an effective adsorbent in the adsorption of methyl violet dye from aqueous solutions. FT-IR, SEM, TGA and XRD analyzes were used to describe the structure of the hydrogels. The effect of adsorption parameters such as temperature, contact time, dye concentration, adsorbent dosage and pH on the adsorption process efficiency was investigated. The Langmuir, Freundlich, Dubinin-Radushkevich (D-R) and Temkin isotherm models were used to describe the equilibrium behavior of adsorption process. Also, to study the kinetic behavior of the process, pseuso-first-order, pseudo-second-order and Elovich models were used. In addition, the thermodynamic behavior of traditional hydrogel samples was investigated.

2. Materials and Methods

2.1. Materials

Methacrylic acid (MAA) and acrylamide (AAm) monomers and methyl violet (MV) dye (λ_{max} = 582 nm) were purchased from Merck (Darmstadt, Germany). Potassium persulfate (KPS) was purchased from Samchun (Seoul, Korea). N,N'-Methylenebisacrylamide (MBA) and bentonite were purchased from Sigma Aldrich (Munich, Germany).

2.2. Preparation of poly(MAA-co-AAm)/Bentonite nanocomposite hydrogels

Free radical polymerization method was used to prepare poly(MAA-co-AAm) and poly(MAA-co-AAm)/Bentonite nanocomposite hydrogels. For copolymerization of monomers in hydrogel synthesis, 5 ml MAA were poured in a three-necked flask equipped with mechanical stirrer, nitrogen gas inlet-outlet and thermometer. The appropriate amount of bentonite (0-15 wt. %) was

dispersed in 2 g of AAm and 10 mL of deionized water, and the mixture was sonicated for 20 min at 25°C to disperse the nanoclay sheets in AAm solution. A mixture of bentonite, AAm and N,N'-Methylenebisacrylamide (MBA) as a crosslinker were added to the three-neck flask and heated with MAA to 70°C during purification with nitrogen gas. After 30 min, a potassium persulfate (KPS) as an initiator was added to the flask to produce free radicals. The gel was formed after 20 min and the reaction was continued for 3 h until the polymerization was completed. In order to remove the non-reactive monomers, the hydrogels were washed several times with deionized water (DW). The nanocomposite hydrogels were dried in an oven at 55°C for 48 h. The dried hydrogels were grinded to 250-500 μm size and kept for further use. Poly(MAA-co-AAm) hydrogel, without bentonite nanaoclay, were synthesized according to the above method for comparison.

2.3. Method of characterization

The chemical structure of monomers (MAA and AAm), bentonite nanoclay, poly(MAA-co-AAm) and poly(MAA-co-AAm)/bentonite nanocomposite hydrogels were investigated by FTIR spectroscopy (Tensor 27, Broker, Germany). The scanning range of the samples was worked by IR spectra from wavenumbers from 400 to 4000 cm^{-1}. X-ray diffraction patterns were obtained using an X-ray diffractometer (Siemens S5000, Germany) at 40 kV and 30 mA equipped with a CuKa radiation source with a scanning speed of 0.2° per minute at ambient temperature. To calculate the base distance (d_{001}) from the silicate layer, the Bragg equation ($n\lambda = 2d\sin\theta$) with λ=1.5418 Å was used [24]. In this XRD analysis, the diffraction angle (2θ) varied from 2-12 degrees. The morphology of the nanocomposite hydrogel surfaces was determined by scanning electron microscopy (SEM) analysis (FE-SEM MIRA3, FEG-SEM, TUSCAN, Czech Republic) equipped with X-ray scattering analysis (EDX). For SEM analysis, samples of poly(MAA-co-AAm) and poly(MAA-co-AAm)/bentonite nanocomposite hydrogels were coated with a gold-plated spray steam. To determine the nanoclay distribution at the cross-section of nanocomposite hydrogels, the main profiles in the sample thickness were obtained by EDXA and dot-mapping (Microanalysis Oxford Instruments model 7718 INCA PentaFET). Thermal stability of primary and nanocomposite hydrogel samples was performed by thermogravimetric analysis (TGA) using Linseis instrument (Linseis N81 A1750, USA) in the temperature range of 25-900°C with heating rate of 10°C/minute under nitrogen atmosphere [25].

To study the adsorption capacity, different concentrations of MV dye (10-100 mg/L) were prepared for evaluation at different concentrations in DW. For this purpose, 0.05 g of dry hydrogel was added to a 250 mL flask containing 50 mL of dye solution. Adsorption experiments were performed on a magnetic stirrer at 800 rpm at 25°C for 60 min. After reaching equilibrium absorption capacity (initial tests were performed at 25°C, contact time of 60 min and weight of 1 g/L of the adsorbent dosage), the solutions were filtered by centrifugation and the amount of dye adsorption was measured using the UV-Vis spectrophotometer (Agilent Technologies, model Cary 100, Santa Clara, CA, USA) at the maximum color emission wavelength. The adsorption capacity of the adsorbents at equilibrium (q_e, mg/L) and adsorption efficiency (R %) were calculated using Eqs. 1 and 2, respectively.

$$R(\%) = \frac{(C_0 - C_t)}{C_0} \times 100 \quad (1)$$

$$q_t = \frac{(C_0 - C_t)V}{m} \quad (2)$$

where, C_0 is the initial concentration of the contaminant, C_t is the final concentration, V is the volume of the solution used, and m (g/L) is amount of adsorbent used.

2.5. Swelling behavior of hydrogels

Swelling behavior of copolymer and nanocomposite hydrogel samples were investigated. For this purpose, 20 mg of adsorbent was poured into 10 mL of DW and after one day (24 hours), the solution was centrifuged. The adsorbent was separated from DW and weighed. The amount of adsorbent swelling ratio was calculated using Eq. 3 [22].

$$\text{Swelling Ratio} = \frac{(W_{wet} - W_{dry})}{W_{dry}} \quad (3)$$

where, W_{wet} and W_{dry} are the weight of wet and dry hydrogel samples, respectively.

3. Results and Discussion

3.1. Properties of hydrogels

Fig. 1a shows the FTIR spectra of the bentonite nanoparticles, which indicating characteristic peaks at wavenumber of 3616 cm^{-1} (corresponding to the tensile vibration of the hydrogen bonds), 1474 and 1596 cm^{-1} (indicating the bending of methylene groups) [26]. The rest of the vibrations are in the range of 1000-1050 cm^{-1} due to the tension of the Si-O-C bond [27]. Figure 1b shows the FTIR spectra of poly(MAA-co-AAm) hydrogel after adsorption of the dye contaminant. The peaks at 1631 and 1699 cm^{-1} indicate the involvement of the carbonyl and vinyl groups of MAA monomer in the free radical polymerization. In addition, the peaks of 1728 and 1751 cm^{-1} are symmetrically bonded to carboxylate anions and C=O tensile vibrations in the monomers, respectively [28]. Figure 1c shows the FTIR spectra of poly(MAA-co-AAm)/bentonite nanocomposites after adsorption of MV dye contaminants. Compared to the shape of the copolymer hydrogel, the vibration distance is reduced, which means that the methyl violet (MV) dye was trapped in the pores of the nanocomposite. In addition, the increase in the transmission spectrum in 1653 cm^{-1}, which is related to the poly(MAA-co-AAm) bonds, indicates that these bonds are filled with dye contaminants. Finally, the peaks in the nanocomposite structure between 400-500 cm^{-1} are related to Si-O-Si and Si-O-Al bond tension [29].

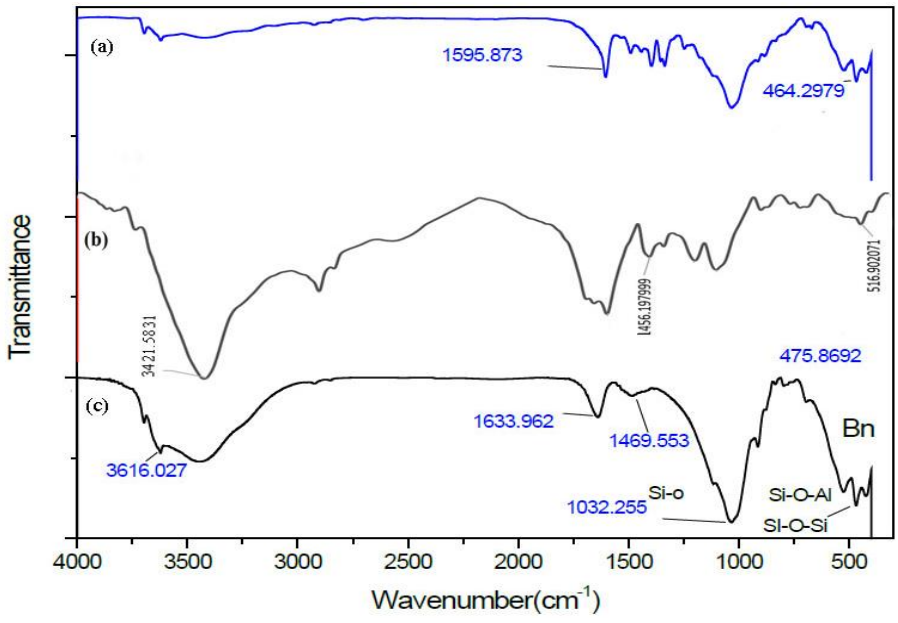

Fig. 1. FTIR results for a) bentonite b) poly(MAA-co-AAm) hydrogel c) poly(MAA-co-AAm)/bentonite nanocomposite hydrogel

Figure 2 shows the XRD patterns of bentonite nanoparticles, poly(MAA-co-AAm), and poly(MAA-co-AAm)/bentonite nanocomposite hydrogels. As shown in the figure, bentonite

nanoclay shows many diffraction peaks due to the presence of different crystalline phases. The distinct peak at 2θ=5-10° (specified in 2θ=5.7°) related to the basal-spacing (d_{001}) for layered gallery structure of bentonite nanoclay. From Bragg's equation for layered silicates such as bentonite nanoclay, the d001 is calculated as 1.55 nm. For poly(MAA-co-AAm) and poly(MAA-co-AAm)/bentonite nanocomposite hydrogels, this distinct peak hasn't appeared which can be due to the complete disaggregation of the bentonite silicate layers during the formation of the nanocomposite structure. This means the complete dispersion of single layers of clay into polymeric matrix occurred. In this case, the exfoliated structure for the resulting nanocomposite is obtained. Also, in the poly(MAA-co-AAm)/bentonite nanocomposite hydrogel XRD pattern, some peaks in 2θ=12.5, 16, and 22° are observed which indicating the lower crystalline structure of these samples [30].

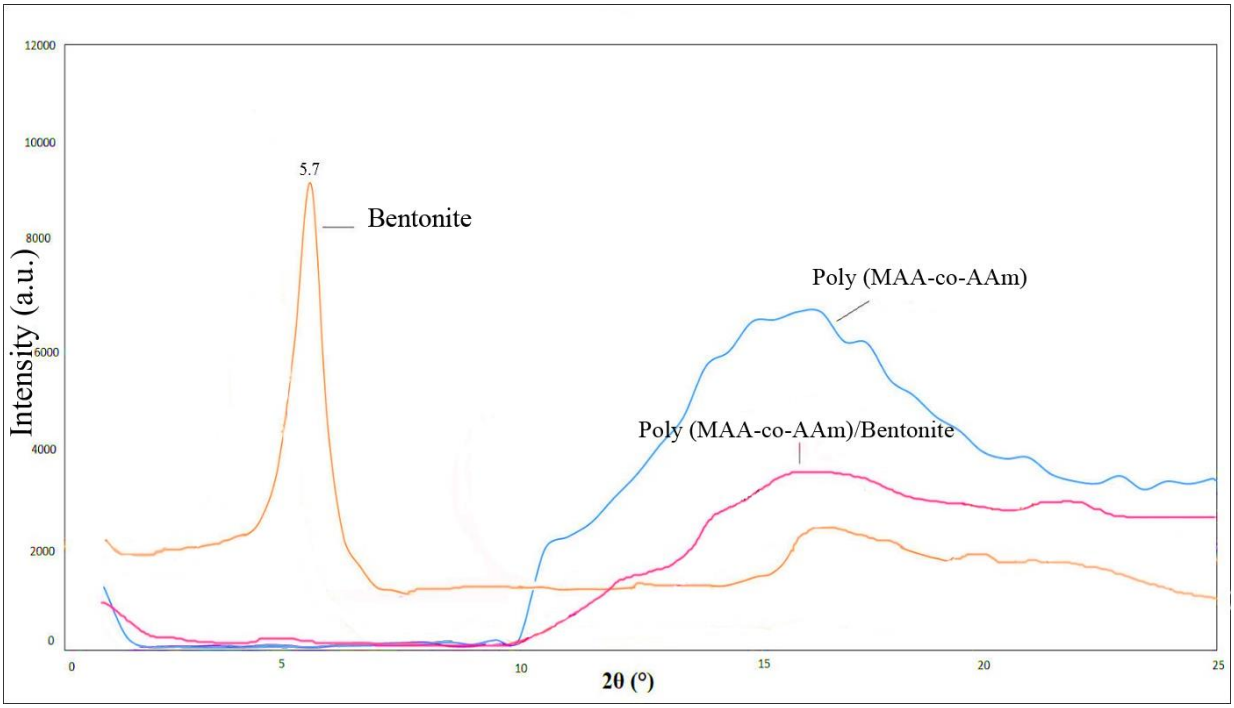

FFig. 2. X-ray diffraction results (XRD) of bentonite, poly(MAA-co-AAm), and poly(MAA-co-AAm)/bentonite nanocomposites

Figure 3 shows the TGA curves of poly(MAA-co-AAm) and poly(MAA-co-AAm)/bentonite nanocomposite hydrogels. Usually, TGA analysis was performed to investigate the thermal stability behavior of poly(MAA-co-AAm) and poly(MAA-co-AAm)/bentonite nanocomposite hydrogels. The results of TGA analysis showed that the weight loss of copolymer and nanocomposite hydrogel samples was done in three stages. The first stage of weight loss occurred

in the range of 50-150 °C temperature, which could be due to the evaporation of water content in the samples. It is noteworthy that at this stage, the weight loss of the nanocomposite sample is more than the copolymer hydrogel sample and this is due to the presence of more water molecules in the structure of the nanocomposite hydrogel. The second stage of weight loss took place in the range of 200-450 °C temperature, where the hydrogels lost a significant part of their weight, which could be related to the destruction of acrylamide bonds as well as the decomposition of excellent monomer compounds. Also at this stage, the C-H bond of methacrylic acid, which is the dominant monomer of the hydrogel, is decomposed. The final weight loss can be due to the decomposition and destruction of the structure of the mentioned materials, which at this stage we see a slight weight loss. As shown in Fig. 3, the addition of bentonite nanoparticles increases the thermal stability of the nanocomposite. In addition, a comparison of the nanocomposite sample with the sample without nanoclay shows that the addition of bentonite nanoclay to the polymeric hydrogel caused a significant increase in the temperature of the nanocomposite during the heating steps. This result may be due to the exfoliated structure that creates strong hydrogen bond interactions with methacrylic acid and acrylamide monomers, evaporating water molecules, destroying the chains and opening the nanocomposite layers.

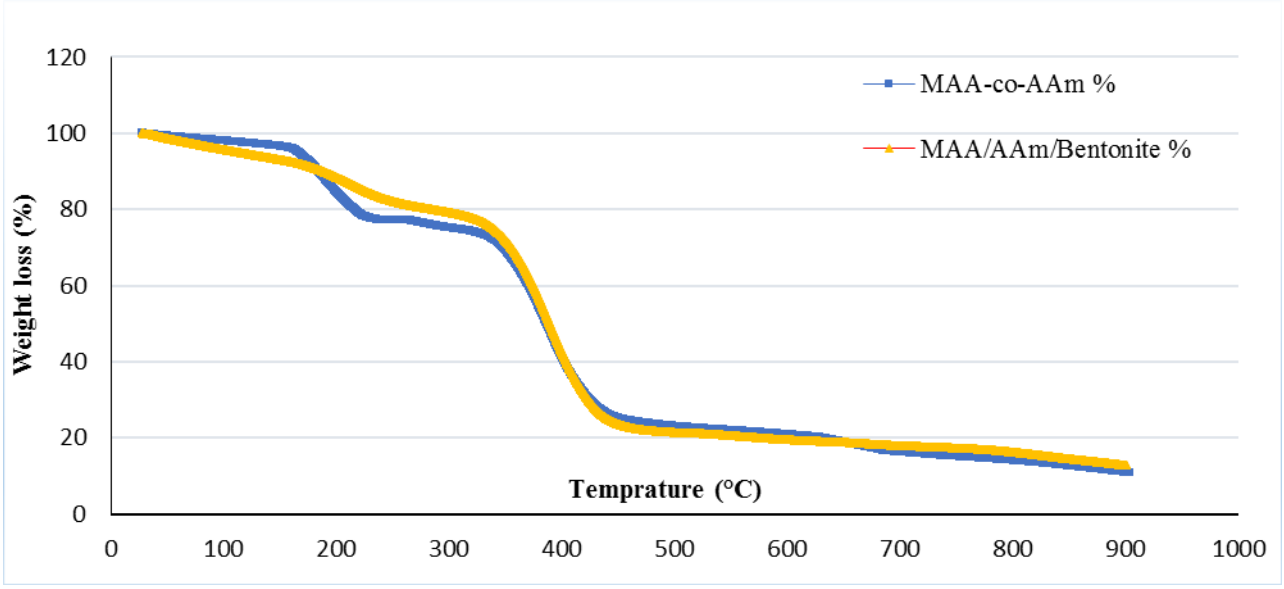

Fig. 3. Comparison of TGA analysis results of poly(MAA-co-AAm) and poly(MAA-co-AAm)/bentonite nanocomposite hydrogels

In order to study morphology and changes in samples of poly(MAA-co-AAm) and poly(MAA-co-AAm)/bentonite nanocomposite hydrogels before and after the methyl violet dye adsorption process, SEM-EDX and dot-mapping analysis were used. Fig. 4 shows the SEM micrographs for poly(MAA-co-AAm) and poly(MAA-co-AAm)/bentonite nanocomposite hydrogels in the dry state. In hydrogels, the amount of swelling depends on the porosity and the average size of the pores. Due to the presence of capillary forces, water is distributed through the pores. As shown in Figure 4b the presence of bentonite nanoparticles increases the porosity of hydrogel and thus, increases the water permeability in the structure of hydrogels. Dot mapping of nanocomposite hydrogels was performed and the distribution of Si element as a marker of nanoparticles in purple dots is shown in Fig. 4c. Preliminary analysis of Si shows the cross-sectional distribution of clay nanoparticles on the nanocomposite hydrogel. As shown in Fig. 4a good distribution of nanoparticles is observed in nanocomposite hydrogel structures. This means that the clay nanoparticles were not accumulated in the hydrogel matrix. Also, after the methyl violet dye adsorption process, the pores and roughnesses on the surface of the composite used were almost saturated, which could be due to the penetration of dye molecules in these pores.

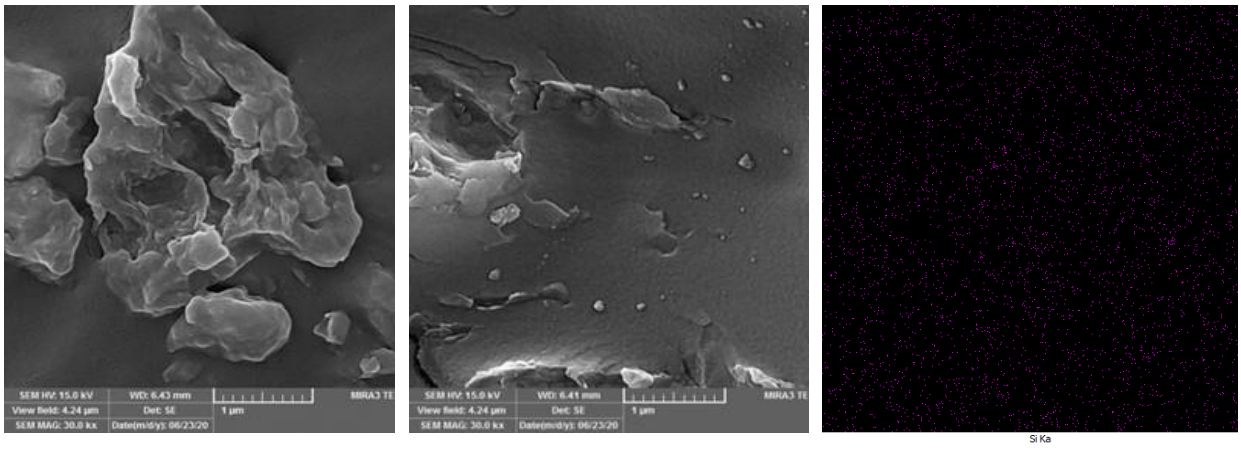

(a) (b) (c)

Figure 4. SEM images of a) poly(MAA-co-AAm) hydrogel, b) poly(MAA-co-AAm)/bentonite nanocomposite hydrogel, and c) dot-mapping of nanocomposite hydrogel

3.2. The effect of different parameters on the adsorption performance

3.2.1. Weight concentration of nanoparticles

Figure 5a shows effect of weight percent of nanoparticles on dye adsorption efficiency. A lower dye adsorption was observed at either low (2.5 wt. %) or high (15 wt. %) of nanoparticles. A highest dye adsorption of 96% was obtained at a nanoparticle weight percent range of 7.5-12.5. It is known that with increasing the weight percentage of bentonite nanoparticles inside the hydrogel, due to the increase of effective surface and active sites, the amount of dye adsorption increased sharply and when the amount of bentonite nanoparticles reached to 12.5 wt. %, due to the accumulation of these nanoparticles inside the hydrogel, the dye adsorption decreases because in this weight percentage, the active sites available for the adsorption process are reduced.

3.2.2. Initial pH

In the adsorption process, the initial pH is an important and effective parameter, because this parameter can affect adsorbent surface ionization and charge [32]. Figure 5b shows the effect of initial pH on dye adsorption efficiency for Poly(MAA-co-AAm) and Poly(MAA-co-AAm)/bentonite nanocomposite hydrogels in the initial pH range of 3 to 10. First, the adsorption efficiency of Poly(MAA-co-AAm)/bentonite was higher than that of Poly(MAA-co-AAm) hydrogels at all pH ranges tested. Second, either at lower (pH< 4) or higher (pH> 9) pH values, the adsorption efficiency was significantly reduced. A highest adsorption rate of 94 and 90% was obtained at pH=7 for Poly(MAA-co-AAm)/bentonite and Poly(MAA-co-AAm) hydrogels, respectively. There are repulsive electrostatic forces between the adsorbent surface and the dye molecules originated from H^+ ions in acidic pH, and OH^- ions in alkaline pH, which reduce the adsorption efficiency [33,34].

3.2.3. Adsorbent dose

The adsorbent dose is another important parameter that affects the adsorption efficiency of contaminants [35]. In this study, the adsorption capacity of Poly(MAA-co-AAm) and Poly(MAA-co-AAm)/bentonite nanocomposite hydrogels was evaluated at an adsorbent dose range of 0.5-4 g/L, an initial dye concentration of 10 mg/L, an initial pH of 7, and a contact time of 60 min. As can be seen from figure 5c, the adsorption efficiency of Poly(MAA-co-AAm)/bentonite nanocomposite hydrogel was higher than that of Poly(MAA-co-AAm) hydrogel at all adsorbent dosages tested. By increasing the adsorbent dose, the adsorption efficiency for both hydrogel types

is increased. This can be explained by an increased contact surface of the adsorbents, which facilitates the adsorption process at a higher concentration. According to the results, with increasing the adsorbent dose from 0.5 to 1.5 g/L, the adsorption efficiency of the dye was increased. Dosage higher than 1.5 g/L did not significantly change the adsorption efficiency of both adsorbent types. This could be due to the reduction of dye concentration in aqueous solution and reduction of active ingredient [36].

3.2.4. The initial concentration of dye

The initial concentration of pollutants in the adsorption process is one of the important factors because it is regarded as a driving force to overcome the mass transfer resistance between solid (adsorbent) phases and aqueous solutions [37]. Figure 5d demonstrates the effect of the initial concentration of dye contaminants on the adsorption efficiency. Increasing the initial dye concentration significantly decreased the adsorption efficiency for both types of adsorbents. At low initial dye concentration, the intermolecular bonds of the dyes are low (10 mg/L), while at high concentrations (100 mg/L) the active sites on the adsorbent surface are completely saturated leaving extra dye molecules unabsorbed [38].

3.2.5. Temperature

Temperature is another effective parameter in the adsorption process because it changes the kinetic energy of molecules, and therefore, affects the adsorption process [20]. To investigate the effect of temperature on the adsorption efficiency, the temperature was changed in the range of 25-45 °C by a thermal heater and the results are shown in figure 5e. It can be seen from this figure that a temperature of 25°C gave the highest adsorption rate (95%). By increasing the temperature, the mobility of the hydrogel side groups increases, causing the adsorbed dye molecules to separate from the hydrogel structure and reduce the adsorption rate. This process indicates that the adsorption reaction is exothermic.

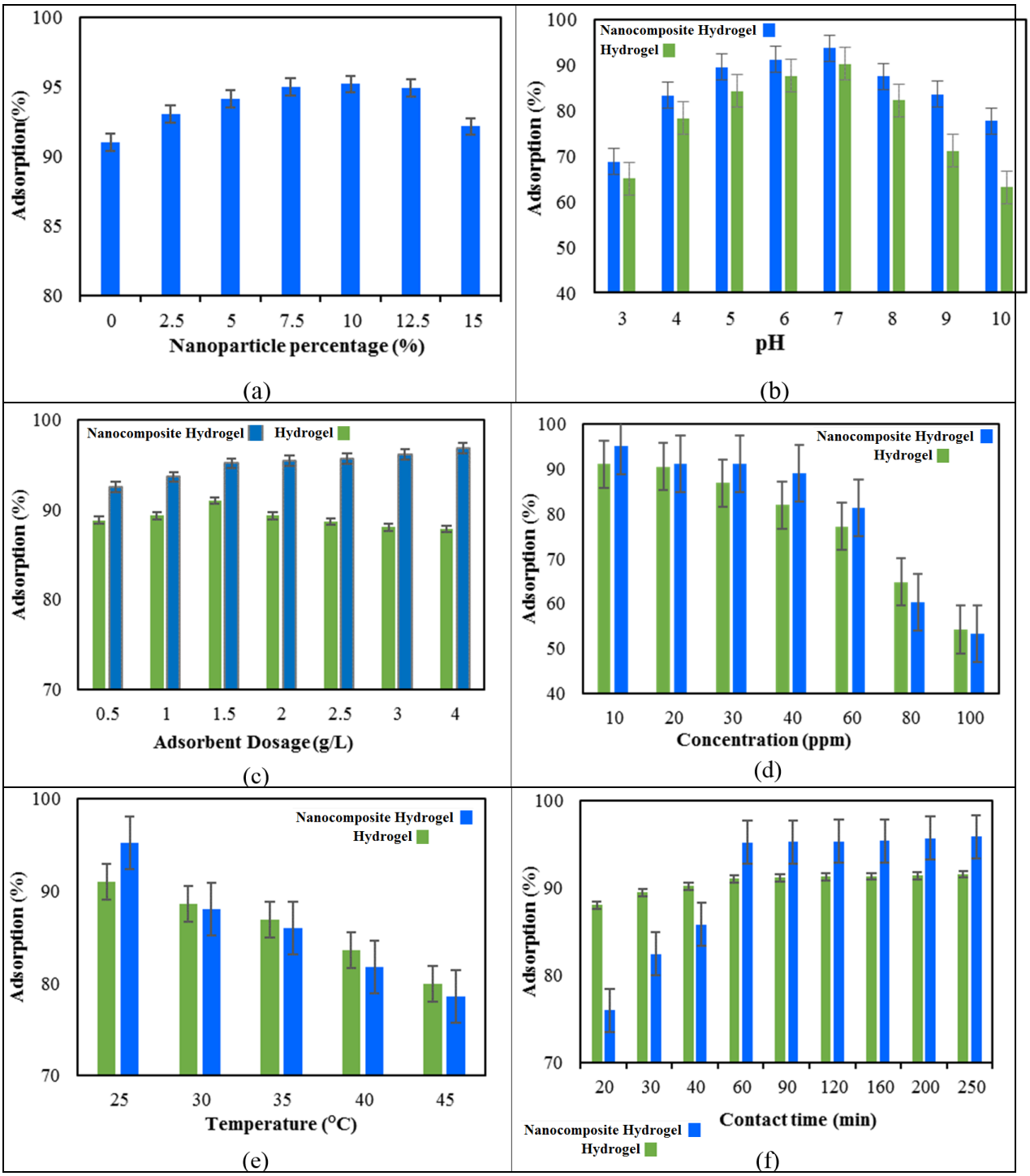

Figure 5. a) Effect of nanoparticle wt. %, b) pH, c) adsorbent dosage, d) the initial concentration of dye (MV), e) contact time, and f) temperature on adsorption efficiency of poly(MAA-co-AAm) and poly(MAA-co-AAm)/bentonite nanocomposite hydrogels. Data are mean of triplicate measurements. Error bars indicate the standard deviation.

3.2.6. Contact time

To evaluate the effect of contact time on the maximum adsorption efficiency of the dye, adsorption at different time intervals (20-250 min), pH=7, adsorbent dose of 1.5 g/L was performed. Figure 5f shows that the adsorption of dyes was faster in the early contact; however, the adsorption rate of the dye was almost constant after 60 min. In the early contact time, there are unoccupied surfaces that are active to absorb the dye. When the contact time increases, the active sites on the adsorbent molecules become saturated decreasing the adsorption rate. According to the results, the optimal time for adsorption of dye contaminants with an initial concentration of 10 mg/L was obtained at 60 min.

3.3. Adsorption isotherm models

Adsorption isotherm models are very important to determine the maximum adsorption capacity of dyes by adsorbents. In the present study, adsorption isotherm models of Langmuir, Freundlich, Dubinin-Radushkevich (D-R), and Temkin were used to evaluate the adsorption behavior of dye contaminants using two types of adsorbent hydrogels. The Langmuir [39], Freundlich [15], D-R [40], and Temkin [22] isotherm models can be expressed according to Eqs. 4, 5, 6, and 7, respectively.

Langmuir: $$q_e = \frac{q_m \,.\, k_l \,.\, C_e}{1 + k_l \,.\, C_e} \quad , \quad R_L = \frac{1}{1 + K_L + C_e} \tag{4}$$

Freundlich: $$q_e = k_f \, C_e^{1/n} \tag{5}$$

D-R: $$q_e = q_m \,.\, \exp\left(- \beta \, \varepsilon^2\right) \quad , \quad \varepsilon = RT \, Ln\left(1 + \frac{1}{C_e}\right) \tag{6}$$

Temkin: $$q_e = B \, Ln\left(A \times C_e\right) \quad , \quad B = \frac{RT}{b_T} \tag{7}$$

where q_m is the maximum adsorption capacity of dye (mg/g), K_L is the Langmuir constant, K_F and n are the Freundlich constants, ε is the Polanyi factor, β reflects the activity coefficient (mol^2/J^2), A (1/g) and b_T (kJ/mol) are Temkin constants, R is the global constant of gases, and T is the absolute temperature (K).

k_L and q_m can be obtained by tracking and tilting the C_e/q_e diagram versus C_e [39]. The dimensionless parameter R_L is one of the important parameters of the Langmuir isotherm model that determines the type of adsorption process. Accordingly, if the values of $R_L > 1$, $R_L = 1$, $R_L = 0$ and $0 < R_L < 1$, the adsorption process is described as undesirable, linear, irreversible and desirable, respectively. The value of the R_L parameter for the MV dye adsorption process was determined using both adsorbents used in the range 0-1, which indicates that the adsorption process using both adsorbents is optimal [15]. By drawing a linear isothermal shape, a constant can be obtained [22]. Figure 6 shows the nonlinear relationship of isotherm models for the process of adsorption of MV dye from aqueous solution using synthesized adsorbents, and the constants and parameters obtained are reported in Table 1. The correlation coefficient (R^2) using the Langmuir isotherm model for the MV dye adsorption process using the Poly(MAA-co-AAm) hydrogel and the Poly(MAA-co-AAm)/Bentonite nanocomposite hydrogel were 0.9965 and 0.9986, respectively. The amount of R^2 determined using the Langmuir isotherm model was higher than other models, indicating that homogeneous surfaces play an important role in the MV dye adsorption process. Also, the value of parameter n for the MV dye adsorption process using Poly(MAA-co-AAm) hydrogels and Poly(MAA-co-AAm)/Bentonite nanocomposite hydrogels were 2.75 and 3.27, respectively, which confirms the optimal and physical adsorption process. The values of A_T and b_T parameters that are determined using the Temkin isotherm show that the interaction between the MV dye and the adsorbent surface has a weak interaction. Therefore, the process of adsorption of MV dye using the desired adsorbents may be physically present. Therefore, the process of adsorption of dye contaminants using the desired adsorbents may be physically present. Parameter ($E = \frac{1}{\sqrt{2\beta}}$) was determined using the D-R isotherm model below 8 KJ/mol, which indicates that the process of adsorption of dye contaminants is physically present [20].

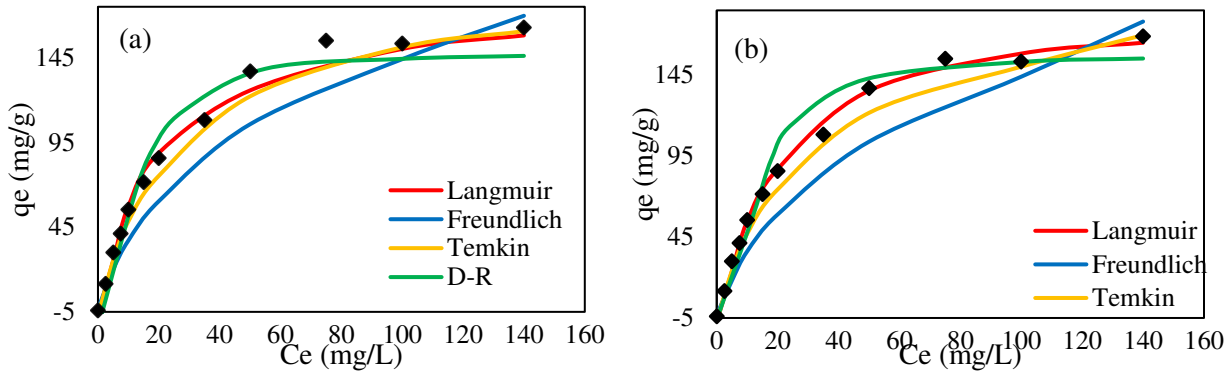

Figure 6. Linear relationship of Langmuir, Freundlich, Temkin, and D-R isotherm models for the adsorption MV dye from aqueous solution using Poly(MAA-co-AAm) hydrogel and Poly(MAA-co-AAm)/bentonite nanocomposite hydrogel.

Table 1. Equilibrium constants and parameters from adsorption process of MV dye

Hydrogel sample	Langmuir		Freundlich		Temkin		Dubinin–Radushkevich (D-R)	
Poly(MAA-co-AAm)	q_m	137.037	n	2.75	B	6.612	E	0.176
	k	0.201	k	10.69	A_T	5.79	q_m	150.45
	R_L	0.014-0.488	R^2	0.8781	R^2	0.9351	β	$4x10^{-6}$
	R^2	0.9965					R^2	0.9214
Poly(MAA-co-AAm)/bentonite Nanaocomposite	q_m	149.32	n	3.27	B	8.077	E	0.372
	k	0.374	k	8.26	A_T	2.34	q_m	174.11
	R_L	0.009-0.338	R^2	0.9287	R^2	0.9844	β	$9x10^{-7}$
	R^2	0.9986					R^2	0.9398

3.4. Thermodynamics study

To describe the thermodynamic behavior of the process of adsorption of dye pollutants from aqueous solution using Poly(MAA-co-AAm) and Poly(MAA-co-AAm)/Bentonite nanocomposite hydrogel from thermodynamic parameters enthalpy (ΔH°), entropy (ΔS°) And Gibbs free energy (ΔG°) was used (Eqs. 8 and 9).

$$\Delta G = - R\ T\ Ln\ (1000 \times K_D) \quad (8)$$

$$\mathrm{Ln}\left(1000 \times K_D\right) = \frac{-\Delta H^{\circ}}{R\,T} + \frac{\Delta S}{R} \qquad (9)$$

where, R is the universal constant of gases (8.314 J/mol.K), T is the absolute temperature (K) and K_D ($K_D = q_e/C_e$) is the equilibrium constant.

To determine the values of ΔH° and ΔS°, the slope and width of the ln K_D versus 1/T diagram were used, respectively (Figure 7) and the calculated parameters are reported in Table 2. The value of the parameter ΔG° for the adsorption of the dye pollutants was determined using both negative adsorbents, indicating that the adsorption process is possible and spontaneous. The ΔH values for the adsorption process using Poly(MAA-co-AAm) and Poly(MAA-co-AAm)/bentonite nanocomposite hydrogels were -61.24 and -36.14 KJ/mol, respectively. ΔH° negative indicates that this process is exothermic in the temperature range 25-45 °C using both adsorbents. The value of the parameter ΔSº was determined for the negative adsorption process, which shows that the random collisions of dye pollutant molecules with the adsorbent surface increase during the adsorption process [20,41].

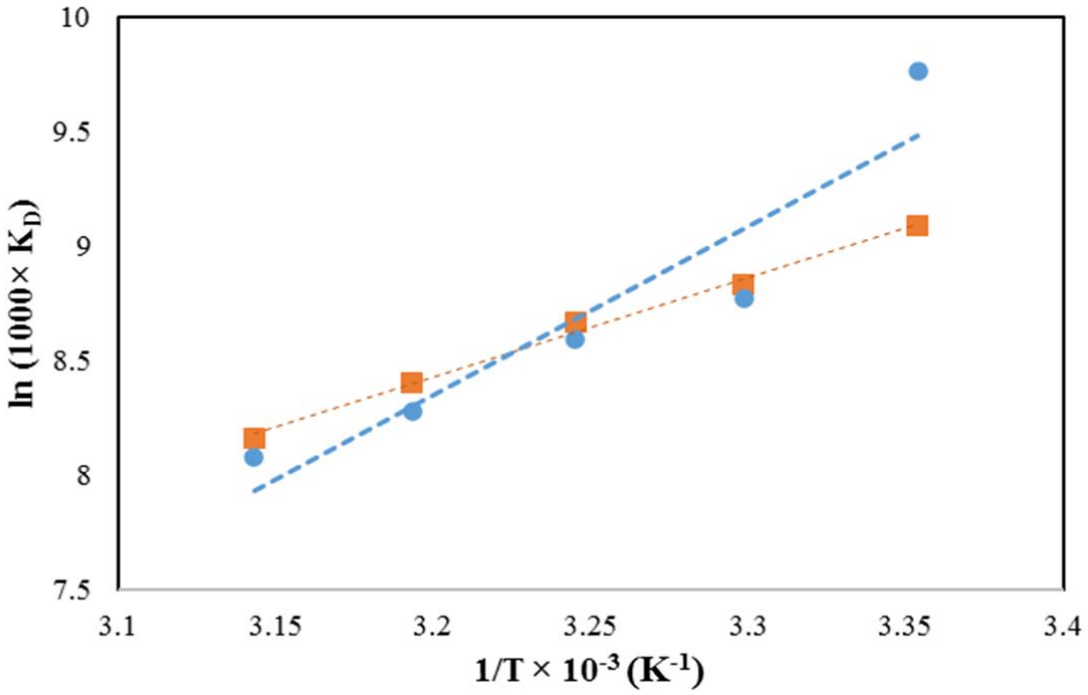

Figure 7. Relation of ln K_D vs. 1/T to determine thermodynamic parameters

Table 2. Thermodynamic constants and parameters for the adsorption process of MV dye using Poly(MAA-co-AAm) hydrogel and Poly(MAA-co-AAm)/Bentonite nanocomposite hydrogel.

Adsorbent)	T (ºC)	ΔG° (KJ/mol)	ΔH° (KJ/mol)	ΔS° (J/mol.K)
Poly(MAA-co-AAm) Hydrogel	25	-24.19	- 61.24	-126.57
	30	-22.09		
	35	-22.01		
	40	-21.54		
	45	-21.36		
Poly(MAA-co-AAm)/bentonite Nanocomposite Hydrogel	25	-22.53	- 36.14	-45.57
	30	-22.25		
	35	-22.20		
	40	-21.88		
	45	-21.58		

3.5. Adsorption Kinetics Study

Kinetic studies provide useful information about the mechanism of the adsorption process. In this study, pseudo-first-order kinetic models, pseudo-second-order, and Elovich kinematic models were used to analyze experimental data. The pseudo-first-order nonlinear model is as follows [41]:

$$q_1 = q_e \left(1 - e^{-kt}\right) \quad (10)$$

and, the pseudo-second-order nonlinear model is as follows [42]:

$$q_2 = \frac{K q_e^2 t}{1 + K q_e t} \quad (11)$$

Also Elovich model is as follows [43]:

$$q_2 = \frac{1}{\beta} \mathrm{Ln}\left(\alpha \beta t\right) \quad (12)$$

where, q_e and q_t (mg/g) show the absorption capacity of equilibrium and the absorption capacity at time t, respectively. k_1 (min^{-1}) and k_2 (g/mg. min) are the speed constants of the pseudo-first-order and pseudo-second-order models, respectively.

The slope and cut of the log diagram (q_{1e} - q_t) in front of t represent k_1 and q_{1e}. In the same way, k_2 and q_{2e} are calculated with graph t/q_t versus t. Experimental data are analyzed using two kinetic models and the parameters are calculated from the above equations and correlation coefficients are obtained. Eq.10 for the pseudo-first-order and Eq.11 for the pseudo-second-order were used to study the kinetics linearly. And the results are shown in Table 3. As can be seen from figure 8 and table 3 and the value of R^2, the pseudo-second-order for Poly(MAA-co-AAm) and Poly(MAA-co-AAm)/bentonite nanocomposite hydrogels have better and closer results to experimental results. Generally, the pseudo-second-order kinetic model has a correlation coefficient and adsorption compared to other models. Considering the values of q_{t2} and k_2 parameters and matching the data with the pseudo-second-order kinetic model, the process of MV dye adsorption may be followed by a combined physical and chemical mechanism, but there is a basic chemical style. The α parameter values for the adsorption process of MV dye using Poly(MAA-co-AAm) hydrogel and Poly(MAA-co-AAm)/bentonite nanocomposite hydrogels were determined to be 0.4276 mg/g.min and 22.15 mg/g, respectively, this indicates that the composite produced has a high adsorption value.

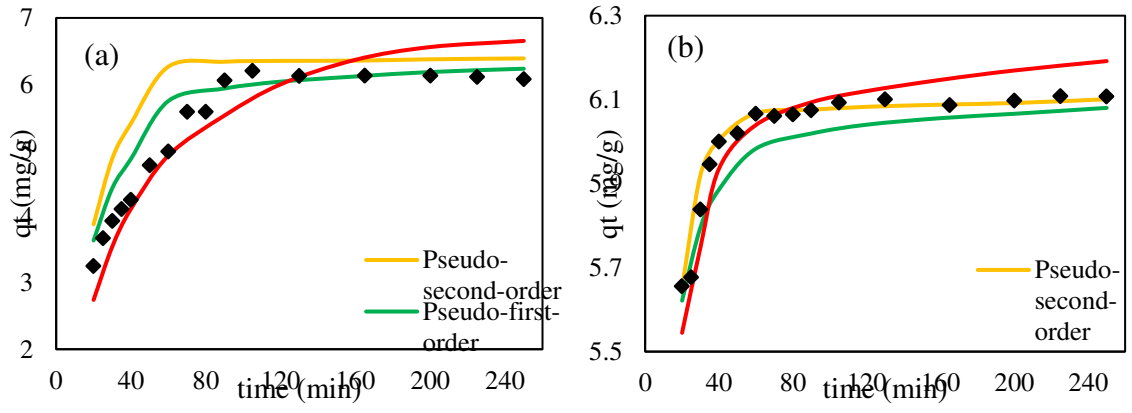

Figure 8. Nonlinear relationship of kinetic models to determine the kinetic parameters of the adsorption process MV dye using Poly(MAA-co-AAm) hydrogel and Poly(MAA-co-AAm)/bentonite nanocomposite hydrogels.

Table3. Kinetic constants and parameters determined for the adsorption process of MV dye.

Hydrogel sample	Pseudo-first-order Model	Pseudo-second-order Model	Elovich Model

Poly(MAA-co-AAm) Hydrogel	q_t	5.33	q_t	18.699	α	0.4276
	K_1	0.012	K_2	0.341	β	0.219
	R^2	0.925	R^2	0.932	R^2	0.876
Poly(MAA-co-AAm)/bentonite Nanaocomposite Hydrogel	q_t	6.069	q_t	17.639	α	22.15
	K_1	0.165	K_2	0.433	β	0.436
	R^2	0.816	R^2	0.977	R^2	0.9042

4. Conclusions

Dyes and pigments are the main pollutants in wastewater streams of various industries. FTIR analysis showed that amide and carboxylate groups are present in the structure of adsorbents that can play an important role in the process of MV dye adsorption. SEM analysis also showed that using MMT nanoparticles, the surface pores of the Poly(MAA-co-AAm) hydrogel system increased dramatically, which could be effective in absorbing MV dye. The Langmuir, Freundlich, D-R and, Temkin isotherm models were examined as equilibrium behaviors. The results showed that the the Langmuir model is more capable than other models. Single-layer adsorption capacity parameter values were determined using Langmuir model (q_{max}) for Poly(MAA-co-AAm) and Poly(MAA-co-AAm)/bentonite nanocomposite hydrogels at 137.037 and 149.32 mg/g, respectively. In addition, the parameters n, R_L and, E determined using isothermal models showed that the MV dye adsorption process is physical and desirable. Also, the A_T and b_T values of the parameter determined using the Temkin isotherm showed that the interaction of the adsorbent surface with the MV dye molecule is weak and the adsorption process can be physical. The determined kinetic data have a good agreement with the quasi-second-order kinetic model and the quasi-second-order kinetic model has a higher correlation coefficient and absorption capacity than other models. By considering the values of the n, R_L, and E parameters and matching the data with quasi-second-order kinetics, the process of MV dye adsorption may be followed by a combined physical-chemical mechanism. The thermodynamic parameters determined for the MV adsorption process showed that the adsorption process is spontaneous and exothermic and the interaction of the adsorbent surface with MV dye increases in the temperature range of 25-45 °C.

References

1. Mittal, H.; Babu, R.; Alhassan, S.M. Utilization of gum xanthan based superporous hydrogels for the effective removal of methyl violet from aqueous solution. *Int. J. Biol. Macromol.* **2020**, *143*, 413–423.

2. Wadhera, P.; Jindal, R.; Dogra, R. Synthesis of semi interpenetrating network hydrogel [(GrA-Psy)-cl-Poly (AA)] and its application for efficient removal of malachite green from aqueous solution. *Polym. Eng. Sci.* **2019**, *59*, 1416–1427.

3. Eskhan, A.; Banat, F.; Selvaraj, M.; Abu Haija, M. Enhanced removal of methyl violet 6B cationic dye from aqueous solutions using calcium alginate hydrogel grafted with poly (styrene-co-maleic anhydride). *Polym. Bull.* **2019**, *76*, 175–203, doi:10.1007/s00289-018-2378-y.

4. Beyranvand, N.S.; Samiey, B.; Tehrani, A.D.; Soleimani, K. Graphene oxide–cellulose nanowhisker hydrogel nanocomposite as a novel adsorbent for methylene blue. *J. Chem. Eng. Data* **2019**, *64*, 5558–5570.

5. Sharma, G.; Kumar, A.; Sharma, S.; Ala'a, H.; Naushad, M.; Ghfar, A.A.; Ahamad, T.; Stadler, F.J. Fabrication and characterization of novel Fe0@ Guar gum-crosslinked-soya lecithin nanocomposite hydrogel for photocatalytic degradation of methyl violet dye. *Sep. Purif. Technol.* **2019**, *211*, 895–908.

6. Gadisa, B.T.; Appiah-Ntiamoah, R.; Kim, H. Amorphous iron sulfide nanowires as an efficient adsorbent for toxic dye effluents remediation. *Environ. Sci. Pollut. Res.* **2019**, *26*, 2734–2746.

7. Foroutan, R.; Mohammadi, R.; Ramavandi, B. Elimination performance of methylene blue, methyl violet, and Nile blue from aqueous media using AC/$CoFe_2O_4$ as a recyclable magnetic composite. *Environ. Sci. Pollut. Res.* **2019**, *26*, 19523–19539.

8. Mallakpour, S.; Tabesh, F. Tragacanth gum based hydrogel nanocomposites for the adsorption of methylene blue: Comparison of linear and non-linear forms of different adsorption isotherm and kinetics models. *Int. J. Biol. Macromol.* **2019**, *133*, 754–766.

9. Mittal, H.; Morajkar, P.P.; Al Alili, A.; Alhassan, S.M. In-situ synthesis of ZnO nanoparticles using gum arabic based hydrogels as a self-template for effective malachite green dye adsorption. *J. Polym. Environ.* **2020**, *28*, 1637–1653.

10. Thakur, S.; Verma, A.; Sharma, B.; Chaudhary, J.; Tamulevicius, S.; Thakur, V.K. Recent developments in recycling of polystyrene based plastics. *Curr. Opin. Green Sustain. Chem.* **2018**, *13*, 32–38.

11. Kaur, K.; Jindal, R. Comparative study on the behaviour of Chitosan-Gelatin based Hydrogel and nanocomposite ion exchanger synthesized under microwave conditions towards photocatalytic removal of cationic dyes. *Carbohydr. Polym.* **2019**, *207*, 398–410.

12. Verma, A.; Thakur, S.; Mamba, G.; Gupta, R.K.; Thakur, P.; Thakur, V.K. Graphite modified sodium alginate hydrogel composite for efficient removal of malachite green dye. *Int. J. Biol. Macromol.* **2020**, *148*, 1130–1139.

13. Rabipour, M.; Pour, Z.S.; Sahraei, R.; Ghaemy, M.; Jazi, M.E.; Mlsna, T.E. pH-Sensitive Nanocomposite Hydrogels Based on Poly (Vinyl Alcohol) Macromonomer and Graphene Oxide for Removal of Cationic Dyes from Aqueous Solutions. *J. Polym. Environ.* **2020**, *28*, 584–597.

14. Al-Aidy, H.; Amdeha, E. Green adsorbents based on polyacrylic acid-acrylamide grafted starch hydrogels: the new approach for enhanced adsorption of malachite green dye from aqueous solution. *Int. J. Environ. Anal. Chem.* **2020**, 1–21.

15. Pakdel, P.M.; Peighambardoust, S.J. Review on recent progress in chitosan-based hydrogels for wastewater treatment application. *Carbohydr. Polym.* **2018**, *201*, 264–279.

16. Sharma, K.; Kumar, V.; Kaith, B.S.; Kumar, V.; Som, S.; Kalia, S.; Swart, H.C. Synthesis, characterization and water retention study of biodegradable Gum ghatti-poly (acrylic acid–aniline) hydrogels. *Polym. Degrad. Stab.* **2015**, *111*, 20–31.

17. Yetimoğlu, E.K.; Kahraman, M. V; Ercan, Ö.; Akdemir, Z.S.; Apohan, N.K. N-vinylpyrrolidone/acrylic acid/2-acrylamido-2-methylpropane sulfonic acid based hydrogels: synthesis, characterization and their application in the removal of heavy metals. *React. Funct. Polym.* **2007**, *67*, 451–460.

18. Pakdel, P.M.; Peighambardoust, S.J. A review on acrylic based hydrogels and their applications in wastewater treatment. *J. Environ. Manage.* **2018**, *217*, 123–143.

19. Foroutan, R.; Peighambardoust, S.J.; Peighambardoust, S.H.; Pateiro, M.; Lorenzo, J.M. Adsorption of Crystal Violet Dye Using Activated Carbon of Lemon Wood and Activated Carbon/Fe_3O_4 Magnetic Nanocomposite from Aqueous Solutions: A Kinetic, Equilibrium and Thermodynamic Study. *Mol.* 2021, *26*.

20. Peighambardoust, S.J.; Aghamohammadi-Bavil, O.; Foroutan, R.; Arsalani, N. Removal of malachite green using carboxymethyl cellulose-g-polyacrylamide/montmorillonite nanocomposite hydrogel. *Int. J. Biol. Macromol.* **2020**, *159*, 1122–1131,

doi:https://doi.org/10.1016/j.ijbiomac.2020.05.093.

21. Moharrami, P.; Motamedi, E. Application of cellulose nanocrystals prepared from agricultural wastes for synthesis of starch-based hydrogel nanocomposites: Efficient and selective nanoadsorbent for removal of cationic dyes from water. *Bioresour. Technol.* **2020**, *313*, 123661.

22. Abdolhosseinzadeh, M.; Peighambardoust, S.J.; Erfan-Niya, H.; Pakdel, P.M. Swelling and auramine-O adsorption of carboxymethyl cellulose grafted poly (methyl methacrylate)/Cloisite 30B nanocomposite hydrogels. *Iran. Polym. J.* **2018**, *27*, 807–818.

23. da Silva, R.C.; de Aguiar, S.B.; da Cunha, P.L.R.; de Paula, R.C.M.; Feitosa, J.P.A. Effect of microwave on the synthesis of polyacrylamide-g-chitosan gel for azo dye removal. *React. Funct. Polym.* **2020**, *148*, 104491.

24. Wang, G.; Shen, J.; Liu, S.; Jiang, C.; Qin, X. Three-dimensional modeling and analysis of macro-pore structure of coal using combined X-ray CT imaging and fractal theory. *Int. J. Rock Mech. Min. Sci.* **2019**, *123*, 104082.

25. Nzioka, A.M.; Kim, M.-G.; Hwang, H.-U.; Kim, Y.-J. Kinetic study of the thermal decomposition process of municipal solid waste using TGA. *Waste and Biomass Valorization* **2019**, *10*, 1679–1691.

26. Ibrahim, W.M.; Hassan, A.F.; Azab, Y.A. Biosorption of toxic heavy metals from aqueous solution by Ulva lactuca activated carbon. *Egypt. J. basic Appl. Sci.* **2016**, *3*, 241–249.

27. Chrzanowska, E.; Gierszewska, M.; Kujawa, J.; Raszkowska-Kaczor, A.; Kujawski, W. Development and characterization of polyamide-supported chitosan nanocomposite membranes for hydrophilic pervaporation. *Polymers (Basel).* **2018**, *10*, 868.

28. Khan, S.A.; Siddiqui, M.F.; Khan, T.A. Synthesis of poly (methacrylic acid)/montmorillonite hydrogel nanocomposite for efficient adsorption of amoxicillin and diclofenac from aqueous Environment: kinetic, isotherm, reusability, and thermodynamic investigations. *ACS omega* **2020**, *5*, 2843–2855.

29. Youssef, A.M.; Al-Awadhi, M.M.; Akl, M.A. Solid phase extraction and spectrophotometric determination of methylene blue in environmental samples using bentonite and acid activated bentonite from Egypt. *J. Anal. Bioanal. Tech.* **2014**, *5*, 1.

30. P. Taylor, “Particulate Science and Technology : An Use of FTIR Spectroscopy in the Characterization of Natural and Treated Nanostructured Bentonites (Montmorillonites) Use of FTIR Spectroscopy in the Characterization of Natural and Treated Nanostructured Bentonites,” no.

September 2014, pp. 37–41, 2012.

31. Koosha, M.; Hamedi, S. Intelligent Chitosan/PVA nanocomposite films containing black carrot anthocyanin and bentonite nanoclays with improved mechanical, thermal and antibacterial properties. *Prog. Org. Coatings* **2019**, *127*, 338–347.

32. David, M.K.; Okoro, U.C.; Akpomie, K.G.; Okey, C.; Oluwasola, H.O. Thermal and hydrothermal alkaline modification of kaolin for the adsorptive removal of lead (II) ions from aqueous solution. *SN Appl. Sci.* **2020**, *2*, 1–13.

33. Forutan, R.; Ehsandoost, E.; Hadipour, S.; Mobaraki, Z.; Saleki, M.; Mohebbi, G. Kinetic and equilibrium studies on the adsorption of lead by the chitin of pink shrimp (Solenocera melantho). *Entomol. Appl. Sci. Lett* **2016**, *3*, 20–26.

34. Rahimi, K.; Mirzaei, R.; Akbari, A.; Mirghaffari, N. Preparation of nanoparticle-modified polymeric adsorbent using wastage fuzzes of mechanized carpet and its application in dye removal from aqueous solution. *J. Clean. Prod.* **2018**, *178*, 373–383.

35. Atangana, E. Adsorption of Zn (II) and Pb (II) ions from aqueous solution using chitosan cross-linked formaldehyde adsorbent to protect the environment. *J. Polym. Environ.* **2019**, *27*, 2281–2291.

36. García, F.E.; Plaza-Cazón, J.; Montesinos, V.N.; Donati, E.R.; Litter, M.I. Combined strategy for removal of Reactive Black 5 by biomass sorption on Macrocystis pyrifera and zerovalent iron nanoparticles. *J. Environ. Manage.* **2018**, *207*, 70–79.

37. Hajizadeh, H.; Peighambardoust, S.J.; Peighambardoust, S.H.; Peressini, D. Physical, mechanical and antibacterial characteristics of bio-nanocomposite films loaded with Ag-modified SiO_2 and TiO_2 nanoparticles. *J. Food Sci.* **2020**, *85*, 1193-1202.

38. Agnihotri, S.; Singhal, R. Effect of sodium alginate content in acrylic acid/sodium humate/sodium alginate superabsorbent hydrogel on removal capacity of MB and CV dye by adsorption. *J. Polym. Environ.* **2019**, *27*, 372–385.

39. Ahmadi, A.; Foroutan, R.; Esmaeili, H.; Tamjidi, S. The role of bentonite clay and bentonite clay@$MnFe_2O_4$ composite and their physico-chemical properties on the removal of Cr(III) and Cr(VI) from aqueous media. *Environ. Sci. Pollut. Res.* **2020**, *27*, 14044–14057, doi:10.1007/s11356-020-07756-x.

40. Shafiee, M.; Foroutan, R.; Fouladi, K.; Ahmadlouydarab, M.; Ramavandi, B.; Sahebi, S. Application of oak powder/Fe_3O_4 magnetic composite in toxic metals removal from aqueous solutions. *Adv.*

Powder Technol. **2019**, *30*, 544–554, doi:https://doi.org/10.1016/j.apt.2018.12.006.

41. Sabbagh, F.; Khatir, N.M.; Karim, A.K.; Nazari, Z.; Jaberi, R. Mechanical Properties and Swelling Behav- ior of Acrylamide Hydrogels using Mont- morillonite and Kaolinite as Clays. **2019**, *7*, 211–219.

42. Sarı, A.; Tuzen, M. Equilibrium, thermodynamic and kinetic studies on aluminum biosorption from aqueous solution by brown algae (Padina pavonica) biomass. *J. Hazard. Mater.* **2009**, *171*, 973–979.

43. Largitte, L.; Pasquier, R. A review of the kinetics adsorption models and their application to the adsorption of lead by an activated carbon. *Chem. Eng. Res. Des.* **2016**, *109*, 495–504.